CHEMISTRY OF MATERIALS
Cite This: Chem. Mater. 2019, 31, 4524−4535
Article
pubs.acs.org/cm

van der Waals Epitaxial Growth and Interfacial Passivation of Two-Dimensional Single-Crystalline Few-Layer Gray Arsenic Nanoflakes

Yi Hu,[†] Zheng-Hang Qi,[†] Jingyu Lu,[†] Renpeng Chen,[†] Mingzhi Zou,[†] Tao Chen,[†] Wenjun Zhang,[†] Yanrong Wang,[†] Xiaolan Xue,[†] Jing Ma,*[,†] and Zhong Jin*[,†,‡]

[†]Key Laboratory of Mesoscopic Chemistry of MOE, Jiangsu Key Laboratory of Advanced Organic Materials, School of Chemistry and Chemical Engineering, Nanjing University, Nanjing 210023, China

[‡]Shenzhen Research Institute of Nanjing University, Shenzhen 518063, China

Supporting Information

ABSTRACT: Numerous theoretical simulation works have predicted the fantastic properties of arsenene, such as a tunable band gap, topological states, and a high carrier mobility. However, the experimental synthesis of two-dimensional arsenic materials is still difficult. Herein, we report the epitaxial growth of single-crystalline few-layer gray arsenic nanoflakes with hexagonal and half-hexagonal shapes via a van der Waals epitaxy method. The gray arsenic nanoflakes can be transferred from mica to other substrates without structural damage. Moreover, a universal method for estimating the antidegradation efficiency of polymer-passivated gray arsenic nanoflakes by determining the interfacial interaction energies and geometry changes via first-principles calculations was developed. Consistent with theoretical predictions, we further experimentally confirm that functional polymer coating can effectively suppress the chemical degradation and phase transformation of gray arsenic nanoflakes for at least 50 days under ambient exposure, thus facilitating further nanodevice fabrication, preservation, and measurements. Moreover, the gray arsenic nanoflakes show metal to semiconductor transformation after long-term ambient exposure owing to the oxidation of arsenic in air.

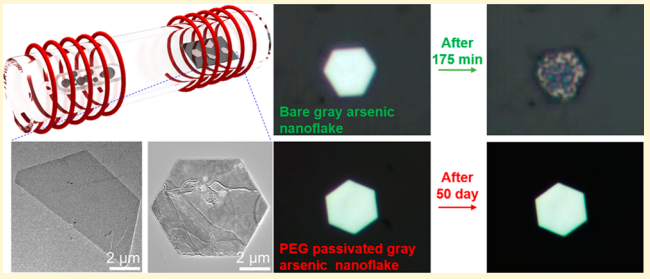

INTRODUCTION

Since the first isolation of graphene in 2004, two-dimensional (2D) materials have attracted a great deal of attention owing to the tremendous potential applications and fantastic electrical and optical properties.[1,2] Monoelemental group IVA 2D materials beyond graphene, such as silicene, germanene, and stanene, have been investigated by theory and experiment.[3−5] However, the very narrow band gaps of group IVA 2D materials limit the applications in nanoelectronic technology. Layered transition metal dichalcogenides (TMDs) show good on−off characteristics for field effect transistors (FETs) and high photoresponsivity for photodetectors, while the relatively low carrier mobilities restrict further industrial applications.[6] As an essential member group of the 2D material family, monoelemental group VA 2D crystals, including phosphorene, arsenene, antimonene, and bismuthene, have recently emerged and attracted significant research interests.[7−9] The tunable band gap and high carrier mobility enable black phosphorene that is appropriate for electrical technology.[7,10] In addition, a phosphorus-substituted black $As_{1-x}P_x$ thin layer with a small band gap showed intriguing performance for infrared (IR) sensing, and the passivation of black $As_{1-x}P_x$ FET devices could lead to the significant improvement of long-term air stability compared to that of air-exposed black $As_{1-x}P_x$.[11,12]

As the congeners of phosphorene, other group VA 2D crystals, including arsenene, antimonene, and bismuthene, have also been theoretically calculated to be promising semiconductors with a tunable band gap and a high carrier mobility.[13,14] Field effect transistors using monolayer arsenene and antimonene as channels have been simulated by a first-principles method, showing a good performance compliant with industry requirements.[15] The optimized sub-10 nm arsenene and antimonene FETs can fulfill the low power requirements of the International Technology Roadmap for Semiconductors in 2028.[16,17] Lu et al. demonstrate that the Fermi level pinning effect of arsenene devices can be reduced by contact with 2D graphene to suppress metal-induced gap states.[18] Besides theoretical predictions, some experimental approaches, such as mechanical exfoliation,[19] liquid exfoliation,[20,21] van der Waals epitaxy,[22] and molecular beam epitaxy,[23−25] have been explored to achieve group VA 2D materials. However, to the best of our knowledge, the experimental realizations of arsenene are merely demonstrated in several recent articles.[21,26] Monolayer and few-layer black arsenic crystals were recently realized via the exfoliation of natural minerals, exhibiting thickness-dependent carrier transfer and in-plane anisotropy in FETs.[27,28] An aqueous shear exfoliation method was developed to fabricate As, Sb, and Bi nanosheets with large scale yields,[21] while the irregular granular

Received: March 22, 2019
Revised: May 27, 2019
Published: May 28, 2019

DOI: 10.1021/acs.chemmater.9b01151
Chem. Mater. 2019, 31, 4524−4535

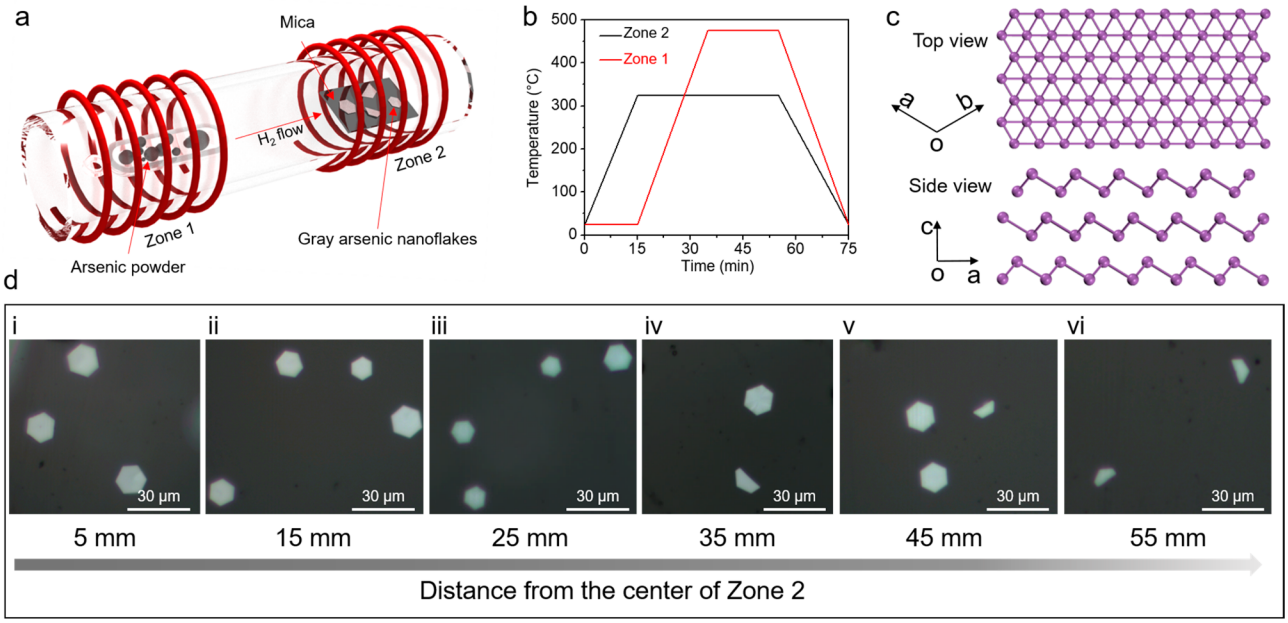

Figure 1. Epitaxial growth of single-crystalline few-layer gray arsenic nanoflakes on the mica substrate. (a) Schematic illustration of a two-zone tube furnace configuration for the growth of gray arsenic nanoflakes. (b) Temperature evolution curves of zone 1 and zone 2 as a function of time during the van der Waals epitaxy process. (c) Top view and side view of the atomic structure of rhombohedral-phase arsenene in orthographic mode. (d) Typical optical images of as-synthesized gray arsenic nanoflakes collected upstream to downstream of the mica substrate.

shapes, relatively large thickness, and small crystal domains are inconvenient for device fabrication. A plasma-assisted process was also reported to synthesize multilayer arsenene, which shows a morphology of nanoribbons on the InAs substrate,[26] but the polycrystalline feature, semiconductive substrate, and buffer layer go against electrical property studies. Hence, the preparation of arsenene or 2D gray arsenic nanoflakes with high crystal qualities and large crystal domains is vital for preventing the studies of arsenene from remaining in the theoretical phase. Moreover, the surface of the arsenic crystal is sensitive to oxygen and humidity under ambient conditions, which seriously hinders the development of fundamental research and practical applications.[29,30] In this case, establishing an effective and extendable strategy to passivate the surface of gray arsenic nanoflakes is also essential for the subsequent studies.

Herein, we report the growth of hexagonal and half-hexagonal few-layer gray arsenic nanoflakes on a mica substrate via van der Waals epitaxy. Mica is an inert and atomically smooth substrate that can directly act as a support for device fabrication and characterization. The as-prepared gray arsenic nanoflakes exhibit an oxygen-free feature with a diagonal length up to 20 μm and a thickness as low as 4 nm and can be easily transferred to other substrates, such as SiO_2/Si substrates and Cu grids free from chemical degradation. Detailed morphology, composition, and structure characterizations confirm the single-crystalline structure of gray arsenic nanoflakes with a rhombohedral phase. Moreover, through theoretical calculations combined with experimental verifications, appropriate polymer candidates can be rationally sorted out to efficiently passivate the surface of gray arsenic nanoflakes. The gray arsenic nanoflakes passivated by polymer coating [such as polyethylene glycol (PEG)] show significantly improved stability for at least 50 days in ambient air, which is conducive to further characterizations and device applications. The transistors based on freshly prepared gray arsenic nanoflakes show a metallic feature, but semiconductive properties will emerge after the environmental degradation of the gray arsenic nanoflakes by ambient air exposure.

EXPERIMENTAL SECTION

Growth of Few-Layer Gray Arsenic Nanoflakes. Single-crystalline few-layer gray arsenic nanoflakes were synthesized by a van der Waals epitaxy method using a two-zone tube furnace system (Figure 1a). Briefly, gray arsenic powder (Aladdin) and freshly exfoliated mica was placed in zone 1 and zone 2 to serve as the precursor and growth substrate, respectively. The tube furnace was first purged by high-purity H_2, and then the flow rate of H_2 was kept at 20 sccm. The temperature of zone 2 was increased and kept at 325 °C (Figure 1b). Subsequently, the temperature of zone 1 was increased to 425 °C over 20 min and held for 20 min to achieve the growth of gray arsenic nanoflakes on mica. After growth, the furnace was cooled to room temperature. The H_2 flow was stopped, and the furnace was purged with high-purity N_2.

Characterizations. Optical images and Raman spectra were recorded in a confocal Raman spectroscope (Horiba, LabRAM Evolution), using a laser with a 633 nm wavelength, a 50× objective lens, a spot size with an ~3 μm diameter, and 1800 lines/mm grating. The laser power was decreased to 3 mW to prevent the samples from suffering from radiation damage. Transmission electron microscopy (TEM) and selected area electron diffraction (SAED) characterizations were performed on a JEM-2100 system with an operating voltage of 200 kV. Topographic atomic force microscopy (AFM) characterizations were performed using a Bruker Dimension Icon instrument. A ScanAsyst model and RTESP probe were used to measure the morphology and thickness of gray arsenic nanoflakes. Scanning electron microscopy (SEM) and energy-dispersive X-ray spectroscopy (EDX) characterizations were conducted on a FEI Nova NanoSEM-450 instrument. X-ray diffraction (XRD) was performed on a powder X-ray diffractometer (Bruker D8 Advance) with Cu Kα irradiation (λ = 1.5406 Å).

Transfer of Few-Layer Gray Arsenic Nanoflakes. The gray arsenic nanoflakes can be transferred to Cu grids or SiO_2/Si substrates. First, the as-synthesized gray arsenic nanoflakes on a mica substrate were spin-coated with a PMMA solution (4 wt % in anisole), followed by annealing at 50 °C for 10 min. Then, the PMMA/gray arsenic/mica

DOI: 10.1021/acs.chemmater.9b01151
Chem. Mater. 2019, 31, 4524−4535

was dipped into boiling deionized water for 10 min until the PMMA/gray arsenic film was completely cleaved from the mica substrate. After being washed three times with deionized water, the PMMA/gray arsenic layers were transferred to TEM grids or SiO_2/Si substrates. Finally, the PMMA layer was removed with acetone and naturally dried in air at room temperature. The transferred nanoflakes were placed in a high-purity N_2-filled container for storage.

Passivation of Few-Layer Gray Arsenic Nanoflakes. PEG, PAN, PMMA, and PVP were separately dissolved in deionized water, *N*-methyl pyrrolidone (NMP), anisole, and ethyl alcohol with identical mass fractions (4 wt %), respectively. The polymer solutions were spin-coated on the substrates with gray arsenic nanoflakes at a speed of 4000 rpm for 1 min, followed by annealing at 80 °C for 10 min. For the removal of the polymer, the substrates were dipped into the same solvents for 1 min and then rapidly dried with a nitrogen gun.

Computational Details. First-principles calculations were performed with the DMol^3 program in the Materials Studio 7.0 suite.[31] The generalized gradient approximation in the Perdew−Burke−Ernzerhof form (GGA-PBE)[32] was employed to describe the electron exchange and correlation effects with a double-zeta plus polarization function (DNP 4.4) basis set.[33] A DFT-D semiempirical correction with the Grimme method[34] was applied with the PBE functional to account for the dispersion interaction. For the arsenene on the mica substrate, the (001) surface of the mica slab was created by cleaving the bulk cells and the slab was separated in the *z*-direction by a 30 Å vacuum from its periodic images to avoid spurious slab interaction. The whole simulation unit is the 20.776 Å × 17.992 Å × 38.376 Å supercell. We performed fully structural optimization of all adsorbate configurations in which the adsorbates along with the mica layers were allowed to fully relax. The adsorbed arsenene was constructed with 30 arsenic atoms, and the edge was saturated with hydrogen atoms. The distance between the arsenene and mica slab was ∼3.3 Å after optimization. For the adsorption of the polymer on arsenene, a supercell containing (4 × 4) unit cells of the arsenene monolayer with an ∼30 Å vacuum layer was used as a support. The convergence tolerances of energy, force, and displacement for the geometry optimization were 2.0×10^{-5} Ha, 0.004 Ha/Å, and 0.005 Å, respectively. The 1 × 1 × 1 *k*-point grid was used to describe the Brillouin zone for geometric optimization.

The calculations with or without the dipole corrections were performed in the Vienna Ab-initio Simulation Package (VASP). The GGA-PBE functional was also employed, and the zero damping DFT-D3 method of Grimme was applied to account for the dispersion interaction. The cutoff energy for the plain waves was set to be 500 eV, and the convergence for the total energy was 10^{-5} eV. The Monkhorst−Pack (MP) set of 3 × 3 × 1 *k*-points was used to sample the Brillouin zone.

Device Fabrication and Measurements. The source and drain electrode patterns were defined by photolithography (Intelligent Micro Patterning, LLC, SF 100). The Ti/Au (10/50 nm) electrodes were subsequently deposited on the gray arsenic nanoflakes using electron beam deposition (Adnnaotech Corp., TT-6). The electronic characterizations were performed on a probe station system with a Keithley 4200-SCS instrument in air and room temperature.

RESULTS AND DISCUSSION

It is known that bulk arsenic crystals normally have three allotropes, including gray arsenic, yellow arsenic, and black arsenic.[35] Semimetallic gray arsenic, namely β-phase As, is the most stable form of arsenic and has a layered structure consisting of a buckled honeycomb structure in rhombohedral space group *R*3*m* (Figure 1c).[36] The buckled honeycomb layers of gray arsenic are stacked via an ABC stacking arrangement (Figure 1c). Yellow arsenic is an insulator with a tetrahedral crystal structure that consists of four As atoms.[37] Unlike gray arsenic or yellow arsenic that has a pure phase, black arsenic has a more complex crystal structure with amorphous or vitreous characteristics and exhibits a semiconductive feature with a band gap around 1.2 eV.[37] In addition, metastable orthorhombic-phase arsenic in space group *Bmab* was also reported, which is isomorphous with black phosphorus exhibiting a puckered honeycomb structure and a band gap of 0.3 eV.[38] Among these different phases of arsenic, gray arsenic and orthorhombic-phase arsenic have layered crystal structures and have the possibility of forming ultrathin 2D materials by exfoliation or epitaxial growth.[39] Theoretical calculations predicted that the monolayers of both gray arsenic and orthorhombic arsenic are semiconductors with indirect band gaps of 0.831 and 1.635 eV, respectively.[13,39] The weak interlayer interactions and 2D layered structure without dangling bonds enable the growth of gray arsenic on an appropriate substrate via van der Waals epitaxy. However, the growth of gray arsenic may suffer from the formation of different crystalline phases during the evaporation and cooling process.[30,35,40] For example, pure gray arsenic can be obtained at crystallization temperatures above 300 °C, while black arsenic crystals can be obtained between 100 and 200 °C.[40] A mixture of gray arsenic and black arsenic crystals will be formed if the temperature is in the range of 200−300 °C. Moreover, the fast cooling of As vapor can lead to the deposition of yellow arsenic, which will rapidly transform into gray arsenic under light illumination.[41] Therefore, to obtain high-quality 2D gray arsenic nanoflakes, controlling the crystalline conditions is vital during the van der Waals epitaxy process. In this work, a two-zone tube furnace system was used for the preparation of β-phase arsenic nanoflakes. As illustrated in Figure 1a, the β-phase arsenic powder precursor and mica substrates were placed upstream (zone 1) and downstream (zone 2), respectively. Mica was utilized as the van der Waals epitaxy substrate, because its chemical inertness and atomic scale smooth surface can reduce the migration energy barriers of As atoms. Typically, the temperature of zone 2 was first increased to 325 °C over 15 min and the temperature of zone 1 was subsequently increased to 475 °C over 20 min (Figure 1b). During the growth process, the high temperature of zone 1 allowed the arsenic powder to sublimate and migrate downstream with the assistance of H_2 carrier gas. The temperature of zone 2 was kept at 325 °C to ensure the uniform growth of β-phase arsenic and avoid the phase transition (more details are given in the Experimental Section). To investigate the structural stability of arsenene on the mica substrate, the atomic geometry of arsenene on the mica substrate was optimized via first-principles calculations. Both freshly exfoliated mica and synthesized gray arsenic nanoflakes are exposed with (00*n*) crystal planes. As the epitaxial growth of gray arsenic nanoflakes was conducted in a H_2 atmosphere, the edges of arsenene on the mica substrate are saturated with hydrogen atoms during the calculations (more details are provided in the Experimental Section). The optimized structures of arsenene on the mica substrate with a top view and a side view are illustrated in Figure S1, showing no obvious geometry aberrance of arsenene and thus indicating that mica can act as an appropriate substrate for the epitaxial growth of arsenene or 2D gray arsenic nanoflakes.

Figure S2 depicts typical optical images of gray arsenic nanoflakes with different magnifications. The white and regular hexagonal and half-hexagonal flakes correspond to the ultrathin gray arsenic nanoflakes. The well-defined morphology of gray arsenic nanoflakes indicates the good crystallinity of the van der Waals epitaxy process. Figure 1d shows optical images of as-synthesized gray arsenic nanoflakes collected from upstream to downstream of the mica substrate, suggesting hexagonal and half-hexagonal shapes with a diagonal length up to 20 μm. With the increase in the distance from the center of zone 2, the shapes

DOI: 10.1021/acs.chemmater.9b01151
Chem. Mater. 2019, 31, 4524−4535

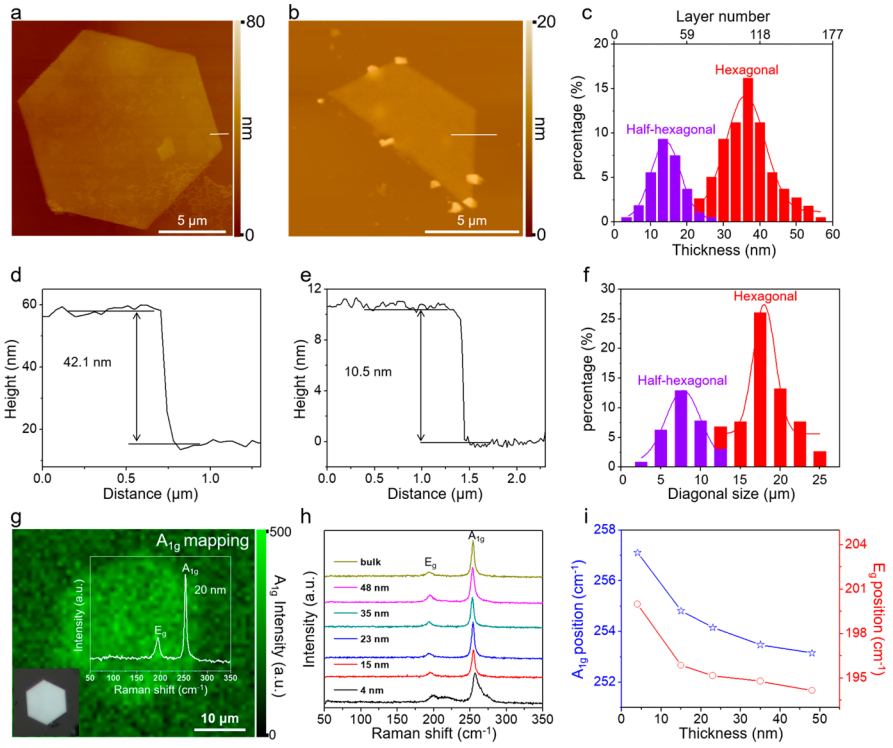

Figure 2. Topographic morphology and Raman spectroscopy analysis of as-grown few-layer gray arsenic nanoflakes. (a and b) AFM images and corresponding height profiles of hexagonal and half-hexagonal gray arsenic nanoflakes. (c) Statistical diagram of the thicknesses of gray arsenic nanoflakes. (d and e) Corresponding height profiles of hexagonal and half-hexagonal gray arsenic nanoflakes in panels a and b, respectively. (f) Statistical histogram of the lateral size distributions of gray arsenic nanoflakes. (g) Raman mapping of the A_{1g} peak intensity of a 20 nm thick hexagonal gray arsenic nanoflake. The inset in panel g shows the corresponding optical image and Raman spectrum of this nanoflake. (h) Individual Raman spectra of gray arsenic nanoflakes (in the thickness range of 4−48 nm) and bulk arsenic, showing the thickness-related A_{1g} and E_g peak positions. (i) Peak position shifts of A_{1g} and E_g modes as a function of nanoflake thickness.

of gray arsenic nanoflakes are gradually varied from hexagons to half-hexagons. The ultrathin half-hexagonal nanoflakes commonly emerge downstream of the substrate. This phenomenon can be attributed to the limitation of boundary layer diffusion,[42] which leads to a relatively insufficient supply and low partial pressure of the As source downstream of the substrate, thus resulting in the diffusion-limited growth of ultrathin half-hexagonal gray arsenic nanoflakes. Control experiments with different growth periods were also performed to synthesize gray arsenic nanoflakes with different diagonal sizes. Figure S3 shows the optical images of gray arsenic nanoflakes with growth periods of 1−25 min. Initially, only small gray arsenic seed crystals could be viewed when the growth time was merely 1 min (Figure S3a). With the growth time was increased, the diagonal size and the thickness of gray arsenic nanoflakes correspondingly increased, because more arsenic vapor was transported from the arsenic precursor (Figure S3a−f). However, the amounts of large black crystals also inevitably increased when the growth time increased, due to the excess supply of the arsenic source. The two control experiments listed above demonstrated that the thickness and diagonal size can be regulated via the experimental parameters. Figure S4 illustrates the optical images of gray arsenic nanoflakes synthesized on Si and SiO_2/Si substrates, indicating that the growth of gray arsenic nanoflakes is realized by a van der Waals epitaxy mechanism rather than traditional epitaxial growth.

Attributed to the weak van der Waals forces between the products and substrate, van der Waals epitaxy can bear large lattice constant mismatches, even if the crystalline symmetries of the products are different with the substrate. XRD characterizations were performed to verify the crystal phase of gray arsenic nanoflakes grown on the mica substrate (Figure S5), confirming that both the hexagonal and half-hexagonal nanoflakes are gray arsenic with a rhombohedral phase (JCPDS PDF Card 05-0632).

To evaluate the topographic morphology and chemical compositions of gray arsenic nanoflakes, SEM and EDX characterizations were performed. Figure S6a shows the SEM image of a typical hexagonal gray arsenic nanoflake with a diagonal length of ∼20 μm. EDX analysis (Figure S6) confirmed the presence of As element, and the corresponding EDX mapping of the As element (Figure S6b) demonstrated the homogeneous distribution of arsenic atoms, indicating the compositional uniformity. In contrast, EDX mapping of the O element depicted a hexagonal shadow at the same location of gray arsenic nanoflakes (Figure S6c). This confirmed that the gray arsenic nanoflake lacks the oxygen element, which is different from the case for the oxygen-containing mica substrate. This phenomenon further verified that the freshly prepared gray arsenic nanoflakes are free from oxidation.

The topographic morphology and height profiles of gray arsenic nanoflakes were also investigated by AFM. Panels a and b of Figure 2 illustrate two typical AFM images of regular hexagonal and half-hexagonal gray arsenic nanoflakes, in which a diagonal length of 9−16 μm can be viewed. It is noteworthy that thicknesses of hexagonal nanoflakes (42.1 nm in Figure 2d) are normally thicker than the half-hexagonal nanoflakes (10.5 nm in Figure 2e). To investigate the thickness and diagonal size

DOI: 10.1021/acs.chemmater.9b01151
Chem. Mater. 2019, 31, 4524−4535

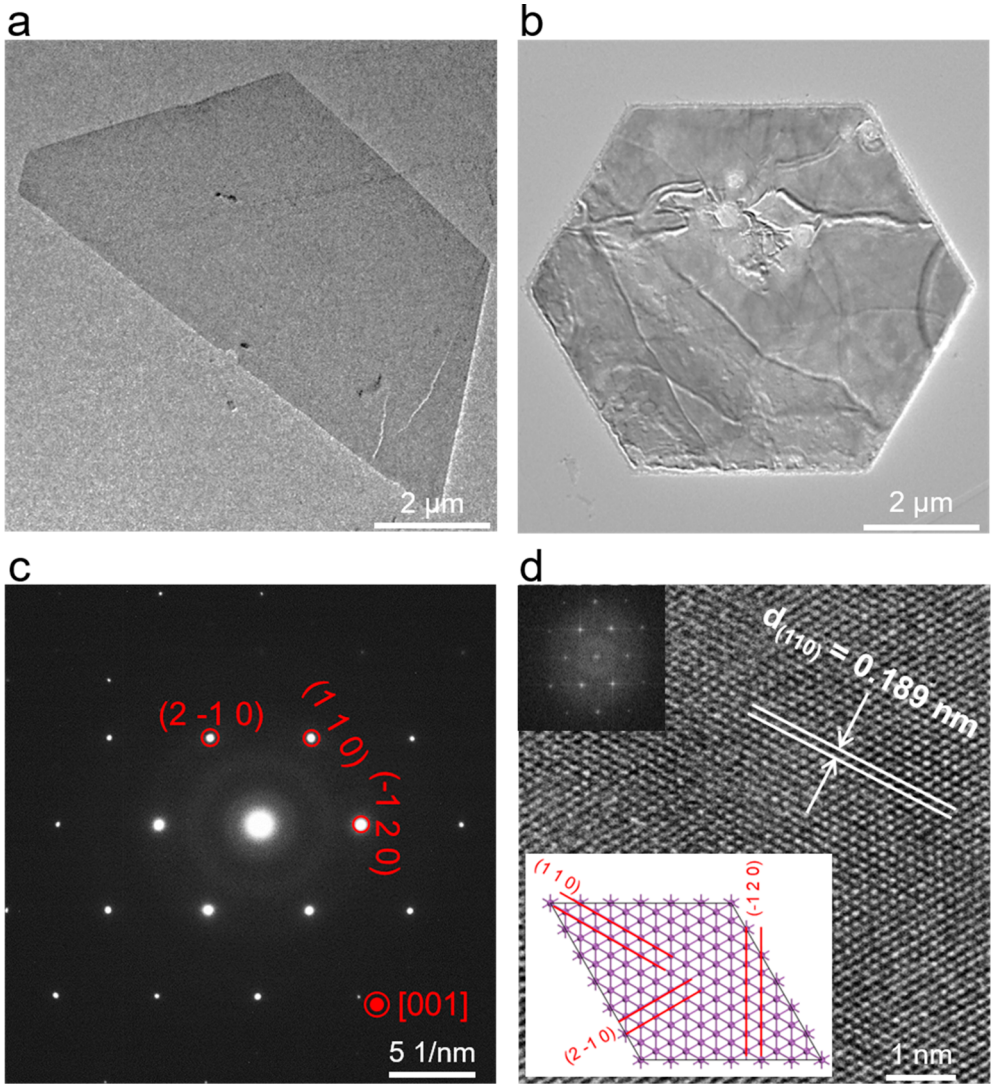

Figure 3. TEM characterizations of as-prepared few-layer gray arsenic nanoflakes. (a and b) TEM images of half-hexagonal and hexagonal gray arsenic nanoflakes, respectively. (c) SAED pattern and (d) HRTEM image collected from panel b, demonstrating the single-crystalline rhombohedral phase. The insets in panel d show the corresponding FFT pattern and the atomic structure of gray arsenic with a $6 \times 6 \times 1$ supercell along the view direction of zone axis (001).

distributions of hexagonal and half-hexagonal gray arsenic nanoflakes, the statistical histograms of thicknesses and lateral sizes were measured from >100 gray arsenic nanoflakes distributed on mica substrates placed at different positions in zone 2. As illustrated in panels c and f of Figure 2, the thickness and lateral size distributions of gray arsenic nanoflakes both show a camelback-like curve. The diagonal sizes of hexagonal gray arsenic nanoflakes are generally larger than those of half-hexagonal gray arsenic nanoflakes (Figure 2f). The two fitted peaks in the thickness distribution histogram are centered at 36 and 13 nm (Figure 2c), which are consistent with the measured average thicknesses of hexagonal and half-hexagonal gray arsenic nanoflakes, respectively. The thicknesses of half-hexagonal and hexagonal gray arsenic nanoflakes ranged from 3.3 to 27 nm and from 23.3 to 57 nm, respectively. According to a previous theoretical prediction,[10] the theoretical thickness of monolayer arsenene is ~0.135 nm and the interlayer distance is ~0.204 nm. Therefore, corresponding layer number ranges of half-hexagonal and hexagonal gray arsenic nanoflakes are calculated to be around 10−80 and 69−168, respectively. The anisotropic ratios of gray arsenic nanoflakes, defined as the ratio of diagonal length and vertical thickness, are calculated to be within the range of 380−1250, indicating the high degree of anisotropic ratio growth. We also found that the gray arsenic nanoflakes would be potentially subjected to surface oxidation if exposed to ambient conditions for a relatively long period of time, leading to a much rougher surface and eventually chemical degradation, as illustrated in Figure S7.

Raman spectroscopy was used as an effective approach to verify the chemical states and crystalline structure of gray arsenic nanoflakes. In particular, the shifts of Raman characteristic frequencies can directly reflect the variation of interlayer van der Waals force for 2D layered materials.[43] Figure 2g shows the typical Raman spectrum and Raman mapping image of the A_{1g} peak intensity of a 20 nm thick hexagonal gray arsenic nanoflake, and the optical image of this nanoflake is provided in the inset of Figure 2g. Two peaks with frequencies of 195.3 and 254.5 cm^{-1} in the Raman spectrum are assigned to the E_g (in-plane vibration) and A_{1g} (out-of-plane vibration) modes of arsenic, respectively. The two Raman characteristic peaks are similar to

DOI: 10.1021/acs.chemmater.9b01151
Chem. Mater. 2019, 31, 4524−4535

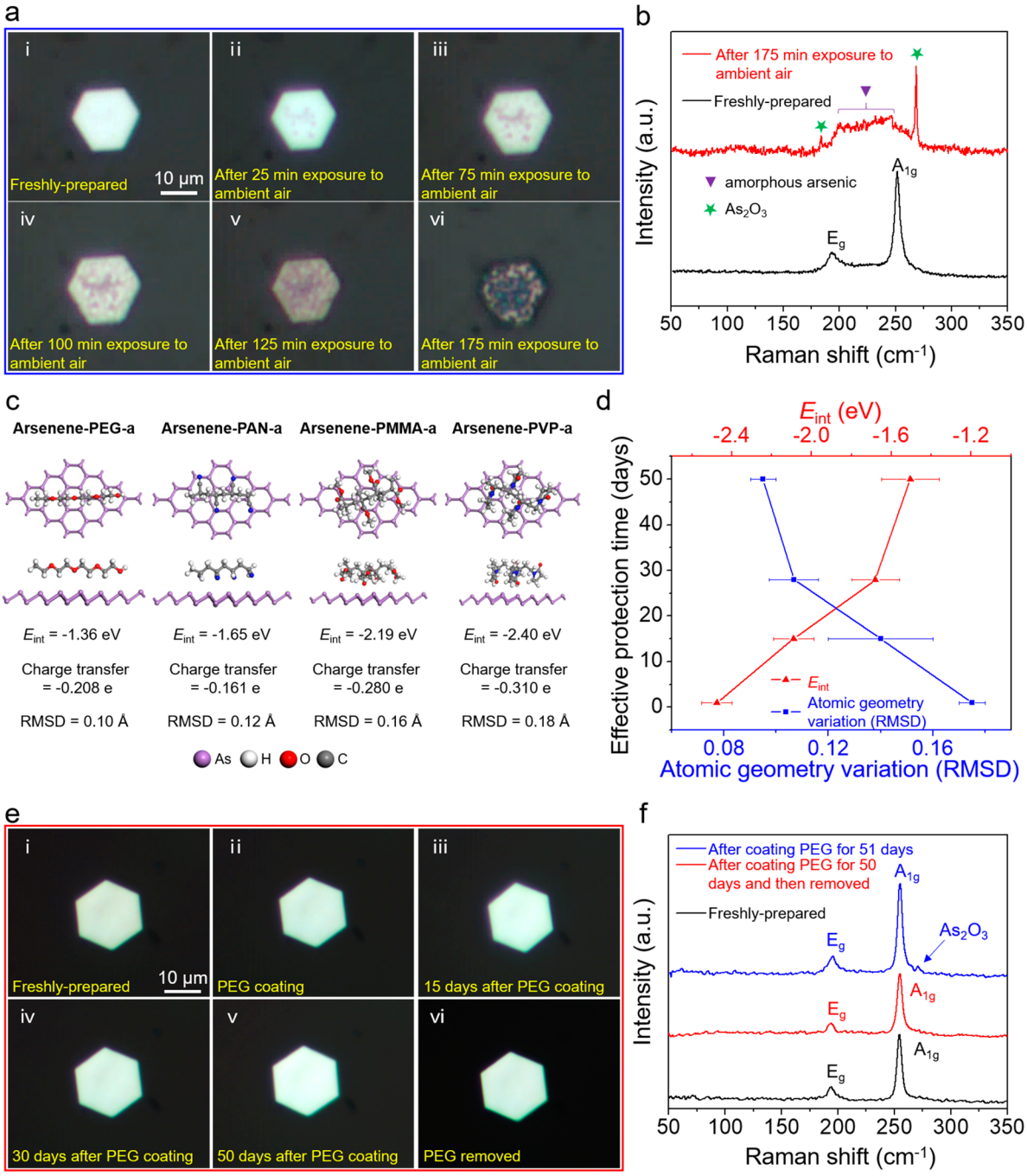

Figure 4. Passivation of few-layer gray arsenic nanoflakes via polymer coating. (a) Optical images of a gray arsenic nanoflake in the freshly prepared state and after exposure to ambient air for different periods of time (25−175 min). (b) Corresponding Raman spectra of the gray arsenic nanoflake in the freshly prepared state (black line) and after exposure to ambient air for 175 min (red line). (c) Simulated top-view and side-view atomic structures of typical PEG-, PAN-, PMMA-, and PVP-coated arsenene. (d) Effective protection time of polymer-coated gray arsenic nanoflakes as a function of interfacial interaction energy (E_{int}) and atomic geometry variation (RMSD). (e) Optical images of a gray arsenic nanoflake in the freshly prepared state, after PEG coating, under the protection of PEG for different periods of time (15−50 days), and after removing PEG. (f) Corresponding Raman spectra of the gray arsenic nanoflake in the freshly prepared state (black line), under the protection of PEG for 51 days (blue line), and under the protection of PEG for 50 days followed by PEG removal (red line).

the previously reported Raman features of gray arsenic with the exposed facet of (001) but with a certain degree of peak position shifts, confirming the synthesized nanoflakes are β-phase arsenic.[44] The corresponding Raman mapping image (Figure 2g) depicts the uniform spatial distribution of A_{1g} signals, indicating the good structural uniformity.

For 2D layered materials, the frequencies of Raman characteristic peaks are commonly related to thickness.[41,45] Figure 2h shows the Raman spectra of gray arsenic nanoflakes with a thickness range of 4−48 nm (as determined by AFM in Figure S8) and also bulk gray arsenic. It is obvious that the positions of both A_{1g} and E_g peaks are strongly dependent on the thickness of gray arsenic nanoflakes. Two additional Raman peaks around 265.2 and 211.4 cm^{-1} emerged when the thickness decreased to 4 nm, which originated from the underlying mica substrate. The positions of A_{1g} and E_g peaks as a function of

DOI: 10.1021/acs.chemmater.9b01151
Chem. Mater. 2019, 31, 4524−4535

thickness are illustrated in Figure 2i. The wavenumbers of both A_{1g} and E_g peaks present a blue-shift tendency when the thickness of gray arsenic nanoflakes decreases. The A_{1g} and E_g peaks of a 48 nm thick gray arsenic nanoflake show almost the same wavenumbers compared to the bulk arsenic crystal. As the thickness decreases from 48 to 4 nm, the wavenumber of the A_{1g} peak correspondingly increases from 253.2 to 257.1 cm^{-1}, and the wavenumber of the E_g peak also increases from 194.2 to 200.0 cm^{-1}. Blue-shifts of Raman frequencies with a decrease in thickness were also found in other 2D materials, which can normally be attributed to the increased lattice constants caused by long-range interlayer Coulombic interactions and structural changes.[22,43,45]

To further study the crystal structure, the gray arsenic nanoflakes were transferred from the mica substrate to SiO_2/Si substrates or Cu grids. Compared to water, arsenic is much more sensitive to oxygen. During the transfer process, the nanoflakes were protected by PMMA and then emerged in boiling deionized water and acetone for a short time rather than during exposure to oxygen. Therefore, the freshly transferred nanoflakes show almost no degradation (Figure 3, Figure S9, and Figure S10). Figure S9a,b exhibit two optical images of hexagonal and half-hexagonal gray arsenic nanoflakes transferred onto the SiO_2/Si substrate, showing the well-preserved morphology without fracture or folding. The corresponding Raman spectrum of a 35 nm thick hexagonal gray arsenic nanoflake shows unaltered Raman features with respect to pristine gray arsenic nanoflakes on the mica substrate (Figure 2h). The gray arsenic nanoflakes were also transferred to Cu grids for TEM characterizations. Figure 3a,b illustrates two typical TEM images of hexagonal and half-hexagonal gray arsenic nanoflakes with diagonal lengths of 11 and 7 μm. For another hexagonal gray arsenic nanoflake transferred on a Cu grid (Figure S10a), the corresponding elemental mapping signal of As shows an even distribution (Figure S10b), and the signal of the O element is very weak (Figure S10c), suggesting that the transferred nanoflake is not obviously degraded. Therefore, we can reasonably infer that the short ambient exposure time during the transfer process leads to very slight surface oxidation of nanoflakes and thus has a minimal influence on the crystal phase and physical properties. The SAED pattern (Figure 3c) collected from Figure 3b depicts hexagonal symmetry characteristics, further demonstrating the single-crystalline feature and rhombohedral phase of as-grown gray arsenic nanoflakes. The calculated zone axis is along the [001] orientation, confirming the epitaxial growth of layered gray arsenic nanoflakes. Figure 3d illustrates the typical HRTEM image and corresponding fast Fourier transform (FFT) pattern of a gray arsenic nanoflake, revealing a periodic spacing of 0.189 nm, which is indexed to the (110) planes of β-phase arsenic. To correlate the lattice fringes observed from HRTEM characterization to the crystal planes in actual gray arsenic nanoflakes, the atomic structure of gray arsenic with a 6 × 6 × 1 supercell along the view direction of zone axis (001) are presented in Figure 3d. The lattice planes are correspondingly marked by red lines, showing identical lattice distances and plane angles with respect to the SAED pattern (Figure 3c).

The bulk arsenic crystal is stable in dry air, but if exposed to humid air, it would be slowly oxidized and eventually form a black surface oxidation layer.[35] Figure 4a shows a series of optical images of a hexagonal gray arsenic nanoflake after being exposed for different periods of time in ambient air. The chemical degradation mainly starts from the edge and some spots in the middle region of the nanoflake (Figure 4a-ii) and subsequently spread to the entire surface (Figure 4a-iv). The oxidized nanoflake first exhibits a deep yellow tarnish (Figure 4a-v), and then the surface turns dark brown after exposure in ambient air for 175 min (Figure 4a-vi). Typical HRTEM images of a hexagonal gray arsenic nanoflake after being exposed to ambient air for 175 min are also presented in Figure S11, showing the degradation at the edge and the surface. Corresponding Raman spectra of gray arsenic nanoflakes before and after exposure in ambient air for 175 min are illustrated in Figure 4b. Compared to that of the freshly prepared gray arsenic nanoflake (black line), the Raman spectrum of ambient-exposed gray arsenic nanoflakes (red line) exhibits two additional Raman peaks at 268.9 and 184.2 cm^{-1} (marked by green stars), which are in accordance with the characteristic Raman peaks of As_2O_3.[46,47] Moreover, a broad band around 200−260 cm^{-1} is observed (marked by purple triangles), which is assigned to amorphous arsenic.[48] To further investigate the variation of the composition and crystal phase of gray arsenic nanoflakes exposed in air, XRD characterizations were performed after ambient exposure for 250 min (Figure S12). The XRD pattern can be indexed to cubic arsenolite (JCPDS PDF Card 36-1490), indicating the oxidation and transformation of As into As_2O_3 after long-term air exposure. These results indicate that upon being exposed to ambient conditions for hours, gray arsenic nanoflakes would undergo chemical and structural degradation and turn into amorphous arsenicand As_2O_3. For sample preservation and further device fabrications, suppressing the chemical degradation of gray arsenic by surface passivation is vital.

Several strategies, such as aryl-diazonium functionalization,[49] AlO_x passivation,[50] and graphene/BN coating,[51] have been employed to prevent the ambient degradation of black phosphorus. However, these passivation approaches are almost irreversible, as removing graphene/BN or AlO_x layers is challenging. In this work, we demonstrate the successful interfacial passivation of gray arsenic nanoflakes by coating them with a layer of a chemically inert, resoluble, and multifunctional polymer. The passivation effects of four polymers, including polyethylene glycol (PEG), polyacrylonitrile (PAN), poly(methyl methacrylate) (PMMA), and polyvinylpyrrolidone (PVP), are first investigated via first-principles calculations with the DMol^3 program in the Materials Studio 7.0 suite[31] (more details are provided in the Experimental Section). Figure 4c and Figure S13 illustrate the top-view and side-view atomic structures of arsenene adsorbed with polymers; a−c indicate the different rotation angles of the polymer on arsenene. The corresponding interfacial interaction energies (E_{int}) and charge transfer between arsenene and polymers are labeled at the bottom of each atomic model. The E_{int} is defined by the following equation:

$$E_{int} = E_{complex} - E_{arsenene} - E_{polymer} \quad (1)$$

where $E_{complex}$ is the total energy of the polymer-coated arsenene and $E_{arsenene}$ and $E_{polymer}$ are the individual energies of pristine arsenene and the isolated polymer molecule, respectively. The charge transfer, defined as the charge difference between the arsenene slab and coated polymer, is estimated by Hirshfeld charge analysis.[52] The negative E_{int} values of different polymer coatings demonstrate the thermodynamically favorable processes of the adsorption of the polymer onto arsenene through van der Waals force. The relatively lower value of the calculated E_{int} indicates the relatively stronger interaction between

DOI: 10.1021/acs.chemmater.9b01151
Chem. Mater. 2019, 31, 4524−4535

Table 1. Comparisons of the Calculated Interfacial Interaction Energy (E_{int}), Charge Transfer, Atomic Geometry Variation (RMSD), and Experimentally Determined Effective Protection Time of Gray Arsenic Nanoflakes Coated with Polymer Molecules at Different Rotation Angles

Polymer layer	Chemical Structure	E_{int} (eV)	Charge transfer (e)	RMSD (Å)	Effective protection time
Polyethylene glycol (PEG)	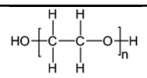	-1.36	-0.208	0.10	50 days
		-1.65	-0.311	0.09	
Polyacrylonitrile (PAN)		-1.65	-0.161	0.12	28 days
		-1.81	-0.226	0.10	
		-1.58	-0.278	0.10	
Polymethyl methacrylate (PMMA)	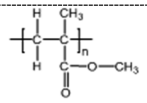	-2.19	-0.280	0.16	15 days
		-1.99	-0.342	0.12	
Polyvinyl pyrrolidone (PVP)		-2.40	-0.310	0.18	1 day
		-2.55	-0.289	0.17	

arsenene and the polymer. The PEG-coated arsenene shows the weakest interfacial interaction with an average E_{int} of −1.51 eV, while the PVP-coated arsenene depicts the strongest polymer−arsenene interaction (average E_{int} of −2.48 eV). These results indicate that PVP intensively interacts with arsenene, while PEG perturbs arsenene the least. Figure S14 compares the atomic geometry differences between pristine arsenene and polymer-coated arsenene through the top views and side views of atomic structures. The root-mean-square deviation (RMSD) of the atomic geometry variation of polymer-coated arsenene relative to pristine arsenene is given in angstroms below each picture. The value of the RMSD can reflect the degree of lattice distortion of polymer-coated arsenene compared to pristine arsenene. The superimposed/overlapped atomic geometries of pristine arsenene and polymer-coated arsenene are also provided in Figure S15, clearly showing the different degrees of in-plane and vertical position distortions of As atoms on polymer-coated arsenene. The most weakly interacting PEG-coated arsenene shows the smallest average value of RMSD (0.095 Å), while the PVP-coated arsenene with the largest absolute average value of E_{int} bears the largest average value of RMSD of 0.175 Å. The average value of RMSD of each polymer-coated arsenene is strongly inversely proportional to the average value of E_{int}, indicating that the stronger interaction between arsenene and the polymer results in a higher degree of lattice distortion and structural instability of arsenene. Actual experiments were also performed to verify the simulated results of individual polymers in stabilizing gray arsenic nanoflakes. The solution of each polymer (including PEG, PAN, PMMA, and PVP) with an identical weight content of 4% is spin-coated on gray arsenic nanoflakes at a rotation speed of 4000 rpm. Panels e and f of Figure 4 and Figure S16 illustrate the optical images and Raman spectra of gray arsenic nanoflakes passivated by PEG, PAN, PMMA, and PVP with different protection periods. The Raman peak evolution of polymer-coated gray arsenic nanoflakes with the same thickness of ∼25 nm was studied. In the Raman spectra of gray arsenic nanoflakes passivated by PEG, PAN, PMMA, and PVP, the Raman peak of As_2O_3 at 269.1 cm^{-1} emerged after 51 days, 29 days, 16 days, and 26 h, respectively, indicating the different protection capability of polymers to gray arsenic nanoflakes. Thus, the effective protection time can be defined as the time difference between the initial polymer coating and the emergence of Raman peaks of As_2O_3. Table 1 lists the calculated interfacial interaction energy (E_{int}), charge transfer, atomic geometry variation (RMSD), and experimentally determined effective protection time of polymer-coated gray arsenic nanoflakes with different rotation angles. It is found that certain polymer coatings can strongly stabilize gray arsenic nanoflakes against chemical degradation under ambient conditions, showing different time lengths of effective protection depending on the interaction between the polymer and gray arsenic nanoflakes. The smallest absolutely average value of E_{int} and the smallest average RMSD of PEG-coated gray arsenic nanoflakes lead to the longest effective protection time of 50 days, whereas the highest absolutely average value of E_{int} and highest average RMSD of PVP-coated gray arsenic nanoflakes result in the shortest effective protection time of 1 day. Figure 4d shows the effective protection time as a function of E_{int} (red line) and RMSD (blue line), indicating that the protective time of polymer coating is associated with the interfacial interaction strength, which can be estimated by the average values of E_{int} and RMSD. The effective protection time increases nearly monotonically with an increase in the average value of E_{int} and decreases monotonically with an increase in the average value of RMSD. To consider the finite charge transfer and its effect on the interfacial interaction energy, the interaction energies with or without the dipole corrections were calculated and compared (more details are provided in the Experimental Section). As shown in Table S1 and Figure S17, the dipole correction has minor effects on the interaction energies, indicating that the results obtained by VASP still support the relation between the interaction energies and antidegradation efficiency of polymer-passivated arsenene. The experimental results are quite consistent with the first-principles calculation results, indicating that the possible polymer candidates can be screened via theoretical simulations to ensure effective interfacial passivation of gray arsenic nanoflakes. Figure 4e illustrates typical optical images of a gray arsenic nanoflake in the freshly prepared state (Figure 4e-i), after coating with PEG and kept for different periods of time in ambient air (Figure 4a-ii-v), and after the removal of PEG (Figure 4e-vi). The gray arsenic nanoflake shows almost unchanged optical contrast and color before and after the ambient exposure for 50 days with the passivation of the PEG coating. The Raman spectra collected from a gray arsenic nanoflake before and after its storage of 50 days protected by PEG exhibit identical Raman features (Figure 4f), such as the

DOI: 10.1021/acs.chemmater.9b01151
Chem. Mater. 2019, 31, 4524−4535

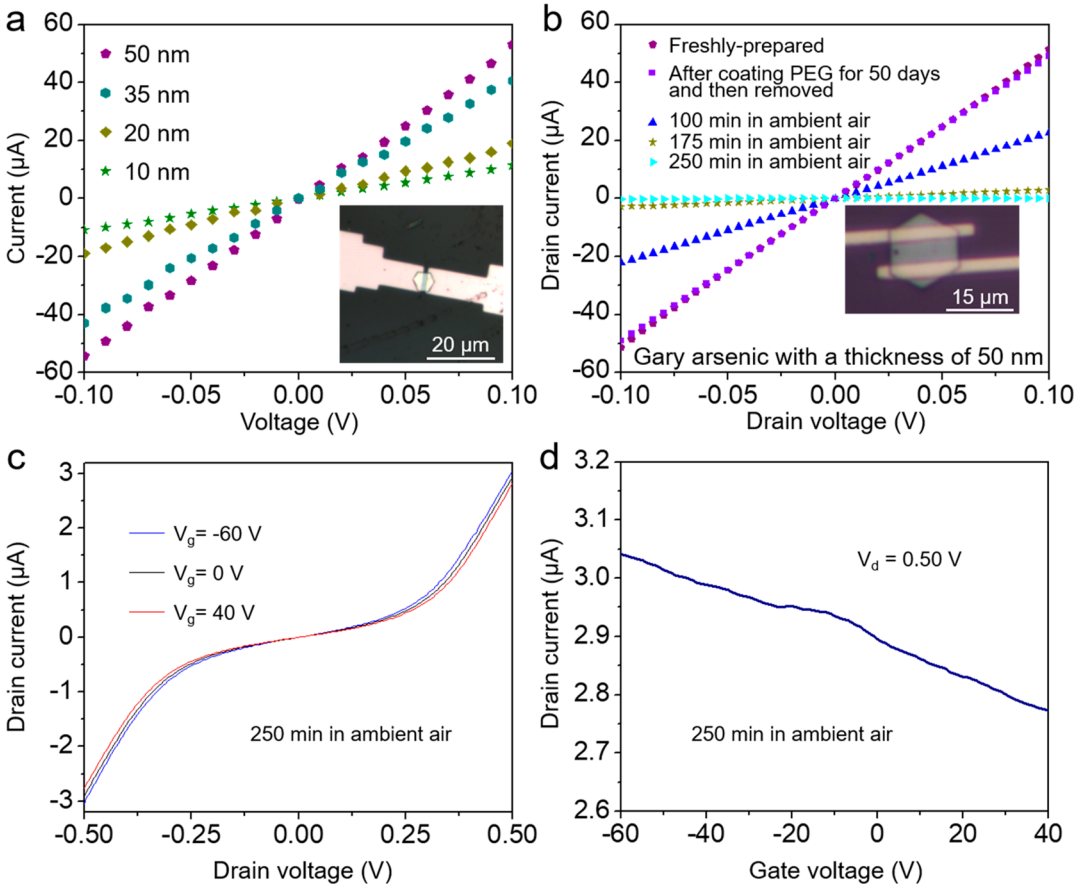

Figure 5. Electrical properties of few-layer gray arsenic nanoflakes. (a) $I-V$ characteristics of freshly prepared gray arsenic nanoflakes with different thicknesses between 10 and 50 nm. The inset shows the optical image of a typical device based on a 35 nm thick hexagonal nanoflake and Ti/Au electrodes on the mica substrate. (b) I_d-V_d characteristics of a 50 nm thick nanoflake after different durations of ambient exposure with or without polymer passivation. The inset presents the optical image of this device with Ti/Au electrodes on the SiO_2/Si substrate. (c) Output characteristic curves of the 50 nm thick nanoflake after a 250 min ambient exposure. (d) Transfer characteristic curve of the 50 nm thick nanoflake after a 250 min ambient exposure with the drain voltage set to 0.5 V.

A_{1g} and E_g peak positions, indicating that PEG can effectively passivate the surface of gray arsenic nanoflakes against ambient degradation.

To further investigate the compositions of the bulk arsenic precursor and freshly prepared and polymer-passivated gray arsenic nanoflakes, systematic XPS characterizations were performed. As illustrated in Figure S18a, no other peaks were detected in the XPS survey spectrum of the bulk arsenic precursor, indicating the precursors are composed of arsenic without obvious impurities. The Al and Si peaks in the XPS survey spectrum of gray arsenic nanoflakes and PEG-passivated gray arsenic nanoflakes originated from the mica substrate. The magnified XPS spectrum of the bulk arsenic precursor shows two peaks located at 42.4 and 41.7 eV, which are assigned to the $3d_{3/2}$ and $3d_{5/2}$ bands of As (Figure S18b), respectively. Compared with bulk arsenic, the $3d_{3/2}$ and $3d_{5/2}$ peaks of gray arsenic nanoflakes show identical shapes, but the positions are shifted to 40.9 and 40.3 eV, respectively (Figure S18c). The peak shifts are consistent with previous XPS characterizations of shear-exfoliated arsenene,[21] in which the XPS peak of the As 3d core level presents a red-shift after being exfoliated into nanosheets. Similar to those of the bulk arsenic precursor and gray arsenic nanoflakes, the XPS spectrum of polymer-passivated gray arsenic nanoflakes (taking as an example PEG-passivated gray arsenic nanoflakes) shows two peaks located at 40.8 and 40.1 eV, indicating that polymer passivation makes no difference in the valence state of arsenic.

To evaluate the electrical properties of gray arsenic nanoflakes and the protection effect of polymer coating, gray arsenic nanoflakes on the mica substrate were contacted by patterned Ti/Au electrodes as shown in the inset of Figure 5a (more details are provided in the Experimental Section). Each gray arsenic nanoflake device has the same channel length of 4 μm and width of 12.5 μm. Figure 5a shows the $I-V$ curves of freshly prepared gray arsenic nanoflakes with a thickness range of 10−50 nm (as determined by AFM analysis in Figure S19). suggesting the thickness-dependent electrical resistance. The electrical conductivity can be calculated by the following equation:

$$\sigma = I_d L / V_d W t \quad (2)$$

where σ is the electrical conductivity, I_d is the drain current, L is the channel length, W is the channel width, t is the thickness of a gray arsenic nanoflake, and V_d is the drain voltage. The calculated electrical conductivity of a 10 nm thick gray arsenic nanoflake is 3.5×10^3 S m^{-1}, suggesting the gray arsenic nanoflakes may potentially act as a conductive component to achieve suitable band alignments in nanoelectronics devices. The calculated electrical conductivity of a typical gray arsenic nanoflake is ~4.5 times smaller than the electrical conductivity of antimonene nanoflakes (1.6×10^4 S m^{-1}).[22] This is because

DOI: 10.1021/acs.chemmater.9b01151
Chem. Mater. 2019, 31, 4524−4535

the metallicity of antimony is stronger than that of arsenic, thus leading to a higher electrical conductivity of antimonene nanoflakes. The $I-V$ curves measured on a 20 nm thick gray arsenic nanoflake with and without the passivation of PEG coating are illustrated in Figure S20a. The $I-V$ curves show the slight decay of electrical performance before and after storage for 50 days with the protection of PEG coating. However, the $I-V$ curves present a dramatic reduction in electrical conductivity before and after the 175 min exposure to ambient air. This result confirms that polymer passivation can effectively suppress the degradation of gray arsenic nanoflakes and the covering and/or removal of PEG has no influence on the electrical performance of gray arsenic nanoflakes. The greatly improved stability of gray arsenic nanoflakes in an ambient environment enabled by the surface passivation of the polymer will facilitate further experimental processes, including device fabrication and characterizations. In this way, the exploration of the intrinsic properties and potential applications of gray arsenic can be promoted. It is also possible to sort out different functional polymers to stabilize gray arsenic nanoflakes and meanwhile endow gray arsenic nanoflakes with various properties. For instance, PMMA with a superior dielectric property can also act as the gate insulator in the nanoelectronic devices of gray arsenic nanoflakes. PVP possesses excellent physiological compatibility, which is convenient for the biological tests of gray arsenic nanoflakes. The alkali and acid resistance of PAN can prolong the preservation of gray arsenic nanoflakes in different environments. The hydrophilic property of PEG can reduce the surface tension between water and gray arsenic nanoflakes.

To study in detail the gate voltage-dependent drain current after different durations of ambient air exposure, the gray arsenic nanoflakes were transferred on SiO_2/Si substrates and fabricated into two-terminus devices. Figure 5b illustrates the typical I_d-V_d curves of a 50 nm thick gray arsenic nanoflake with or without PEG passivation after different durations of ambient exposure. The inset presents the corresponding optical image of this gray arsenic nanoflake-based device. In Figure 5b, the I_d-V_d curves of a 50 nm thick gray arsenic nanoflake show a current decay tendency similar to that of the 20 nm thick gray arsenic nanoflake (Figure S20a). The PEG-passivated 50 nm thick gray arsenic nanoflake also shows a slight decay of electrical conductivity in I_d-V_d curves before and after storage for 50 days. The decreased resistances of gray arsenic nanoflakes with respect to the ambient exposure time indicate the different degrees of oxidation and/or degradation. No gate effect is observed from the freshly prepared gray arsenic nanoflake devices on the SiO_2/Si substrate with the gate voltage ranging from −60 to 40 V (the purple line in Figure S20b), which was mainly attributed to the overlap of the energy levels of a semimetal multilayer gray arsenic nanoflake without a band gap or Dirac cone. This phenomenon is consistent with previous theoretical predictions that the band gap will emerge only in arsenene with single or double atomic layers.[13,39] The gate voltage-dependent drain current curves of this gray arsenic nanoflake device after exposure to ambient air for different periods of time are shown in Figure S20b. The transfer characteristic curve depicts a nearly unchanged drain current during the gate voltage sweep from −60 to 40 V even after the 175 min ambient air exposure (Figure S20b). Interestingly, the drain current of this device after the 250 min ambient exposure presents a slight decrease during the gate voltage sweep from −60 to 40 V under a consistent drain voltage (the cyan line in Figure S20b), indicating the emergence of the gate effect. Panels c and d of Figure 5 illustrate the output and transfer characteristic curves of the gray arsenic nanoflake device after 250 min in ambient air with a magnified vertical scale. The I_d-V_d curve of the gray arsenic nanoflake device after the 250 min ambient air exposure shows apparent Schottky contacts (Figure 5c), which are attributed to the semiconductive behavior of the oxidized gray arsenic nanoflake. The drain currents obviously decrease during the gate voltage (V_g) sweeps from −60 to 40 V, suggesting a p-type semiconducting feature. The oxidation of As into As_xO_y accounts for the semiconductor transition of gray arsenic nanoflakes after a long period of ambient air exposure. The variation of electrical properties after long-term ambient air exposure suggests more potential applications of gray arsenic nanoflakes.

CONCLUSIONS

In summary, we report the van der Waals epitaxial growth of single-crystal few-layer rhombohedral-phase arsenic nanoflakes, which can be transferred from mica to other substrates. Raman spectra of gray arsenic nanoflakes exhibit thickness-dependent evolution of A_{1g} and E_g peak shifts. Moreover, we propose a universal calculation method to evaluate the passivation effect of polymers on arsenene via first-principles calculations, which may be applied to other 2D materials that are unstable under ambient conditions. The gray arsenic nanoflakes show highly improved stability upon exposure to ambient air via polymer coating, enabling the preservation and further device tests. The transistors based on gray arsenic nanoflakes were fabricated and investigated in a freshly prepared state and after ambient air exposure, showing metal to semiconductor transformation. The successful epitaxial growth of gray arsenic may pave the way for further research of 2D arsenic materials, such as the investigation of electronic and biochemical properties for various applications.

ASSOCIATED CONTENT

Supporting Information

The Supporting Information is available free of charge on the ACS Publications website at DOI: 10.1021/acs.chemmater.9b01151.

Density functional theory-calculated atomic structures, geometries, and interfacial interaction energies; additional optical images, XRD patterns, EDS analysis, AFM images, Raman spectra, TEM images, and XPS characterizations of the samples; and results of electrical property measurements (PDF)

AUTHOR INFORMATION

Corresponding Authors

*E-mail: majing@nju.edu.cn.
*E-mail: zhongjin@nju.edu.cn.

ORCID

Jing Ma: 0000-0001-5848-9775
Zhong Jin: 0000-0001-8860-8579

Author Contributions

Z.J. and Y.H. conceived the idea of this study and designed the experiments. Y.H. performed the sample synthesis, AFM characterizations, and data analysis. J.L., R.C., M.Z., T.C., W.Z., Y.W., and X.X. performed the material characterizations. Z.-H.Q. and J.M. performed the theoretical calculation analysis. All of the authors analyzed the data and discussed the results.

DOI: 10.1021/acs.chemmater.9b01151
Chem. Mater. 2019, 31, 4524−4535

Y.H. and Z.J. co-wrote and revised the manuscript. Z.J. and J.M. supervised the project.

Notes

The authors declare no competing financial interest.

■ ACKNOWLEDGMENTS

This work was supported by the National Key R&D Program of China (2015CB659300, 2016YFB0700600, and 2017YFA0208200), projects of the NSFC (21872069, 51761135104, 21673111, and 21573108), the Natural Science Foundation of Jiangsu Province (BK20180008), the High-Level Entrepreneurial and Innovative Talents Program of Jiangsu Province, and the Fundamental Research Funds for the Central Universities.

■ REFERENCES

(1) Novoselov, K. S.; Geim, A. K.; Morozov, S.; Jiang, D.; Zhang, Y.; Dubonos, S. A.; Grigorieva, I.; Firsov, A. Electric Field Effect in Atomically Thin Carbon Films. *Science* **2004**, *306*, 666.

(2) Butler, S. Z.; Hollen, S. M.; Cao, L. Y.; Cui, Y.; Gupta, J. A.; Gutiérrez, H. R.; Heinz, T. F.; Hong, S. S.; Huang, J. X.; Ismach, A. F.; Johnston-Halperin, E.; Kuno, M.; Plashnitsa, V. V.; Robinson, R. D.; Ruoff, R. S.; Salahuddin, S.; Shan, J.; Shi, L.; Spencer, M. G.; Terrones, M.; Windl, W.; Goldberger, J. E. Progress, Challenges, and Opportunities in Two-Dimensional Materials Beyond Graphene. *ACS Nano* **2013**, *7*, 2898.

(3) Fleurence, A.; Friedlein, R.; Ozaki, T.; Kawai, H.; Wang, Y.; Yamada-Takamura, Y. Experimental Evidence for Epitaxial Silicene on Diboride Thin Films. *Phys. Rev. Lett.* **2012**, *108*, 245501.

(4) Dávila, M. E.; Xian, L.; Cahangirov, S.; Rubio, A.; Le Lay, G. Germanene: a Novel Two-Dimensional Germanium Allotrope Akin to Graphene and Silicene. *New J. Phys.* **2014**, *16*, 095002.

(5) Zhu, F. F.; Chen, W. J.; Xu, Y.; Gao, C. L.; Guan, D. D.; Liu, C. H.; Qian, D.; Zhang, S. C.; Jia, J. F. Epitaxial Growth of Two-Dimensional Stanene. *Nat. Mater.* **2015**, *14*, 1020.

(6) Wang, Q. H.; Kalantar-Zadeh, K.; Kis, A.; Coleman, J. N.; Strano, M. S. Electronics and Eptoelectronics of Two-Dimensional Transition Metal Dichalcogenides. *Nat. Nanotechnol.* **2012**, *7*, 699.

(7) Zhang, S. L.; Guo, S. Y.; Chen, Z. F.; Wang, Y. L.; Gao, H. J.; Gómez-Herrero, J.; Ares, P.; Zamora, F.; Zhu, Z.; Zeng, H. B. Recent Progress in 2D Group-VA Semiconductors: from Theory to Experiment. *Chem. Soc. Rev.* **2018**, *47*, 982.

(8) Pumera, M.; Sofer, Z. 2D Monoelemental Arsenene, Antimonene, and Bismuthene: Beyond Black Phosphorus. *Adv. Mater.* **2017**, *29*, 1605299.

(9) Kong, X. K.; Liu, Q. C.; Zhang, C. L.; Peng, Z. M.; Chen, Q. W. Elemental Two-Dimensional Nanosheets Beyond Graphene. *Chem. Soc. Rev.* **2017**, *46*, 2127.

(10) Li, L. K.; Yu, Y. J.; Ye, G. J.; Ge, Q. Q.; Ou, X. D.; Wu, H.; Feng, D. L.; Chen, X. H.; Zhang, Y. B. Black Phosphorus Field-Effect Transistors. *Nat. Nanotechnol.* **2014**, *9*, 372.

(11) Yuan, S.; Shen, C.; Deng, B.; Chen, X.; Guo, Q.; Ma, Y.; Abbas, A.; Liu, B.; Haiges, R.; Ott, C.; Nilges, T.; Watanabe, K.; Taniguchi, T.; Sinai, O.; Naveh, D.; Zhou, C. W.; Xia, F. N. Air-Stable Room-Temperature Mid-Infrared Photodetectors Based on hBN/Black Arsenic Phosphorus/hBN Heterostructures. *Nano Lett.* **2018**, *18* (5), 3172−3179.

(12) Long, M.; Gao, A.; Wang, P.; Xia, H.; Ott, C.; Pan, C.; Fu, Y.; Liu, E.; Chen, X.; Lu, W.; Nilges, T.; Xu, J.; Wang, X.; Hu, W.; Miao, F. Room Temperature High-Detectivity Mid-Infrared Photodetectors Based on Black Arsenic Phosphorus. *Science Adv.* **2017**, *3* (6), No. e1700589.

(13) Zhang, S. L.; Yan, Z.; Li, Y. F.; Chen, Z. F.; Zeng, H. B. Atomically Thin Arsenene and Antimonene: Semimetal-Semiconductor and Indirect-Direct Band-gap Transitions. *Angew. Chem.* **2015**, *127*, 3155.

(14) Zhang, S. L.; Xie, M. Q.; Li, F. Y.; Yan, Z.; Li, Y. F.; Kan, E. J.; Liu, W.; Chen, Z. F.; Zeng, H. B. Semiconducting Group 15 Monolayers: A Broad Range of Band Gaps and High Carrier Mobilities. *Angew. Chem., Int. Ed.* **2016**, *55*, 1666.

(15) Pizzi, G.; Gibertini, M.; Dib, E.; Marzari, N.; Iannaccone, G.; Fiori, G. Performance of Arsenene and Antimonene Double-Gate MOSFETs from First Principles. *Nat. Commun.* **2016**, *7*, 12585.

(16) Sun, X.; Song, Z.; Liu, S.; Wang, Y. Y.; Li, Y.; Wang, W.; Lu, J. Sub-5 nm Monolayer Arsenene and Antimonene Transistors. *ACS Appl. Mater. Interfaces* **2018**, *10* (26), 22363−22371.

(17) Wang, Y.; Huang, P.; Ye, M.; Quhe, R.; Pan, Y.; Zhang, H.; Zhong, H.; Shi, J.; Lu, J. Many-Body Effect, Carrier Mobility, and Device Performance of Hexagonal Arsenene and Antimonene. *Chem. Mater.* **2017**, *29* (5), 2191−2201.

(18) Wang, Y.; Ye, M.; Weng, M.; Li, J.; Zhang, X.; Zhang, H.; Guo, Y.; Pan, Y. Y.; Xiao, L.; Liu, J.; Pan, F.; Lu, J. Electrical Contacts in Monolayer Arsenene Devices. *ACS Appl. Mater. Interfaces* **2017**, *9* (34), 29273−29284.

(19) Ares, P.; Aguilar-Galindo, F.; Rodriguez-San-Miguel, D.; Aldave, D. A.; Diaz-Tendero, S.; Alcami, M.; Martin, F.; GomezHerrero, J.; Zamora, F. Mechanical Isolation of Highly Stable Antimonene under Ambient Conditions. *Adv. Mater.* **2016**, *28*, 6332.

(20) Gibaja, C.; Rodriguez-San-Miguel, D.; Ares, P.; GomezHerrero, J.; Varela, M.; Gillen, R.; Maultzsch, J.; Hauke, F.; Hirsch, A.; Abellan, G.; Zamora, F. *Angew. Chem., Int. Ed.* **2016**, *55*, 14345.

(21) Gusmão, R.; Sofer, Z.; Bouša, D.; Pumera, M. Pnictogen (As, Sb, Bi) Nanosheets for Electrochemical Applications Are Produced by Shear Exfoliation Using Kitchen Blenders. *Angew. Chem., Int. Ed.* **2017**, *56*, 14417.

(22) Ji, J. P.; Song, X. F.; Liu, J. Z.; Yan, Z.; Huo, C. X.; Zhang, S. L.; Su, M.; Liao, L.; Wang, W. H.; Ni, Z. H.; Hao, Y. F.; Zeng, H. B. Two-Dimensional Antimonene Single Crystals Grown by Van Der Waals Epitaxy. *Nat. Commun.* **2016**, *7*, 13352.

(23) Fortin-Deschênes, M.; Waller, O.; Mentes, T. O.; Locatelli, A.; Mukherjee, S.; Genuzio, F.; Levesque, P. L.; Hébert, A.; Martel, R.; Moutanabbir, O. Synthesis of Antimonene on Germanium. *Nano Lett.* **2017**, *17*, 4970.

(24) Shao, Y.; Liu, Z. L.; Cheng, C.; Wu, X.; Liu, H.; Liu, C.; Wang, J.; Zhu, S.; Wang, Y.; Shi, D.; Ibrahim, K.; Sun, J.; Wang, Y.; Gao, H. Epitaxial Growth of Flat Antimonene Monolayer: A New Honeycomb Analogue of Graphene. *Nano Lett.* **2018**, *18*, 2133.

(25) Reis, F.; Li, G.; Dudy, L.; Bauernfeind, M.; Glass, S.; Hanke, W.; Thomale, R.; Schäfer, J.; Claessen, R. Bismuthene on A SiC Substrate: A Candidate for A High-Temperature Quantum Spin Hall Material. *Science* **2017**, *357*, 287.

(26) Tsai, H. S.; Wang, S. W.; Hsiao, C. H.; Chen, C. W.; Ouyang, H.; Chueh, Y. L.; Kuo, H. C.; Liang, J. H. Direct Synthesis and Practical Bandgap Estimation of Multilayer Arsenene Nanoribbons. *Chem. Mater.* **2016**, *28*, 425.

(27) Zhong, M.; Xia, Q.; Pan, L.; Liu, Y.; Chen, Y.; Deng, H. X.; Li, J.; Wei, Z. Thickness-Dependent Carrier Transport Characteristics of a New 2D Elemental Semiconductor: Black Arsenic. *Adv. Funct. Mater.* **2018**, *28* (43), 1802581.

(28) Chen, Y.; Chen, C.; Kealhofer, R.; Liu, H.; Yuan, Z.; Jiang, L.; Suh, J.; Park, J.; Ko, C.; Choe, H. S.; Avila, J.; Zhong, M.; Wei, Z.; Li, J.; Li, S.; Gao, H.; Liu, Y.; Analytis, J.; Xia, Q.; Asensio, M. C.; Wu, J. Black Arsenic: A Layered Semiconductor with Extreme In-Plane Anisotropy. *Adv. Mater.* **2018**, *30* (30), 1800754.

(29) Greenwood, N. N.; Alan, E. *Chemistry of the Elements*; Elsevier, 1984.

(30) Grund, S. C.; Hanusch, K.; Wolf, H. U. Arsenic and Arsenic Compounds. *Ullmann's encyclopedia of industrial chemistry*; VCH, 2008.

(31) *Materials Studio*, version 7.0; Accelrys, Inc.: San Diego, 2013.

(32) Perdew, J. P.; Burke, K.; Ernzerhof, M. Generalized Gradient Approximation Made Simple. *Phys. Rev. Lett.* **1996**, *77*, 3865.

(33) Delley, B. An All-Electron Numerical Method for Solving the Local Density Functional for Polyatomic Molecules. *J. Chem. Phys.* **1990**, *92*, 508.

(34) Grimme, S. Semiempirical GGA-Type Density Functional Constructed with a Long-Range Dispersion Correction. *J. Comput. Chem.* **2006**, *27*, 1787.

DOI: 10.1021/acs.chemmater.9b01151
Chem. Mater. 2019, 31, 4524−4535

(35) Norman, N. C. *Chemistry of Arsenic, Antimony and Bismuth*; Springer, 1997.
(36) Wcykoff, G. M. G. *Crystal Structures*; Wiley: New York, 1963.
(37) Greaves, G. N.; Elliott, S. R.; Davis, E. A. *Adv. Phys.* **1979**, *28*, 49.
(38) Smith, P. M.; Leadbetter, A. J.; Apling, A. J. The Structures of Orthorhombic and Vitreous Arsenic. *Philos. Mag.* **1975**, *31*, 57.
(39) Kamal, C.; Ezawa, M. Arsenene: Two-dimensional Buckled and Puckered Honeycomb Arsenic Systems. *Phys. Rev. B: Condens. Matter Mater. Phys.* **2015**, *91*, 085423.
(40) Pušelj, M.; Ban, Z.; Grdenić, D. On the Allotropy of Arsenic. *Z. Anorg. Allg. Chem.* **1977**, *437*, 289.
(41) Kalendarev, R. I.; Sazonov, A. I.; Rodionov, A. N.; Chikvaidze, G. V.; Eiduss, J. A. Properties of Vapour-Deposited Yellow Arsenic Films at Various Condensation Conditions. *Mater. Res. Bull.* **1984**, *19*, 11.
(42) Li, C.; Huang, L.; Snigdha, G. P.; Yu, Y. F.; Cao, L. Y. Role of Boundary Layer Diffusion in Vapor Deposition Growth of Chalcogenide Nanosheets: The Case of GeS. *ACS Nano* **2012**, *6*, 8868.
(43) Lee, C.; Yan, H.; Brus, L. E.; Heinz, T. F.; Hone, J.; Ryu, S. Anomalous Lattice Vibrations of Single-and Few-Layer MoS_2. *ACS Nano* **2010**, *4*, 2695.
(44) Lannin, J.; Calleja, J.; Cardona, M. Second-Order Raman Ccattering in the Group-Vb Semimetals: Bi, Sb, and As. *Phys. Rev. B* **1975**, *12*, 585.
(45) Li, H.; Zhang, Q.; Yap, C. C. R.; Tay, B. K.; Edwin, T. H. T.; Olivier, A.; Baillargeat, D. From Bulk to Monolayer MoS_2: Evolution of Raman Scattering. *Adv. Funct. Mater.* **2012**, *22*, 1385−1390.
(46) Quagliano, L. G. Detection of As_2O_3 Arsenic Oxide on GaAs Surface by Raman Scattering. *Appl. Surf. Sci.* **2000**, *153*, 240.
(47) Beeman, D.; Lynds, R.; Anderson, M. R. Structural and Vibrational Properties of a Model of Vitreous As_2O_3. *J. Non-Cryst. Solids* **1980**, *42*, 61.
(48) Lannin, J. S. Raman Scattering Properties of Amorphous As and Sb. *Phys. Rev. B* **1977**, *15*, 3863.
(49) Ryder, C. R.; Wood, J. D.; Wells, S. A.; Yang, Y.; Jariwala, D.; Marks, T. J.; Schatz, G. C.; Hersam, M. C. Covalent Functionalization and Passivation of Exfoliated Black Phosphorus via Aryl Diazonium Chemistry. *Nat. Chem.* **2016**, *8*, 597.
(50) Wood, J. D.; Wells, S. A.; Jariwala, D.; Chen, K. S.; Cho, E.; Sangwan, V. K.; Liu, X. L.; Lauhon, L. J.; Marks, T. J.; Hersam, M. C. Effective Passivation of Exfoliated Black Phosphorus Transistors Against Ambient Degradation. *Nano Lett.* **2014**, *14*, 6964.
(51) Doganov, R. A.; O'Farrell, E. C.; Koenig, S. P.; Yeo, Y.; Ziletti, A.; Carvalho, A.; Campbell, D. K.; Coker, D. F.; Watanabe, K.; Taniguchi, T.; Castro Neto, A. H.; Özyilmaz, B. Transport Properties of Pristine Few-Layer Black Phosphorus by Van Der Waals Passivation in an Inert Atmosphere. *Nat. Commun.* **2015**, *6*, 6647.
(52) Hirshfeld, F. L. Bonded-Atom Fragments for Describing Molecular Charge Densities. *Theor. Chim. Acta* **1977**, *44*, 129.

DOI: 10.1021/acs.chemmater.9b01151
Chem. Mater. 2019, 31, 4524−4535